Highly Sensitive Measurements of Methylene Dynamics With a Frequency-Selective Double-Quantum Sideband Method

Jacob Mayer,[a,b] Frédéric A. Perras[a,b]*

[a] Chemical and Biological Sciences Division, Ames National laboratory, Ames, IA 50011, United States
[b] Department of Chemistry, Iowa State University, Ames, IA 50011, United States

*fperras@ameslab.gov

Abstract

Probing the fast dynamics of surface sites using NMR spectroscopy is highly challenging owing to the sites' high dilution and the difficulties often associated with isotopic enrichment. Intra-CH_2 ^{1}H-^{1}H dipolar couplings are ideal probes of motions given that they only involve ^{1}H's and the tensor has a well-defined size and orientation. We introduce a frequency-selective variant of the double-quantum sideband method to measure like-spin ^{1}H-^{1}H dipolar coupling constants. The experiment dramatically reduces the instrument time required to measure dynamically-averaged intra-CH_2 dipolar couplings. We demonstrate the performance of the sequence using silica-supported silanes as model highly-mobile surface species.

Keywords

Dipolar coupling, Nuclear magnetic resonance, Dynamics, Dipolar Recoupling, Fast-MAS

Graphical Abstract

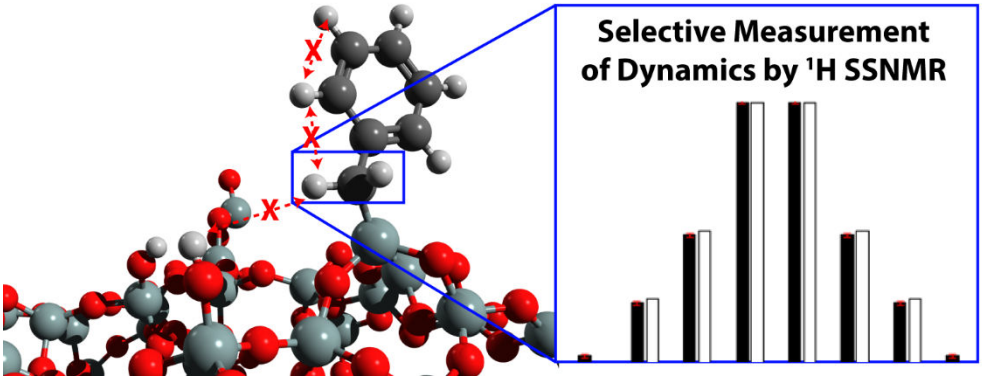

1. Introduction

Structural dynamics play significant roles across fields of chemistry. For instance, transient conformers have been shown to dominate in certain catalytic reactions[1–4]. Flexibility in particular is often associated with enhanced catalytic activity for both heterogeneous and enzymatic systems as this grants them the ability to stabilize intermediate and transition state structures [5–8]. These processes require fast femto to microsecond dynamics that have long posed a challenge to quantify experimentally. Enzyme dynamics are best probed using established nuclear magnetic resonance (NMR) spectroscopy methods [9,10], however, these are not readily transferable to heterogeneous catalyst sites that are more dilute and costly to isotopically enrich.

Anisotropic NMR interactions such as chemical shift anisotropy (CSA), quadrupolar coupling, and dipolar coupling are highly prized for their ability to reveal dynamic motions with atomic and spatial resolution. Given that their magnitude depends on the orientation of a moiety relative to the magnetic field, molecular motions lead to controlled averaging that can be used to elucidate the types of dynamics that are present [11]. The gold standard anisotropic interaction for measuring dynamics is the ^{2}H quadrupolar coupling tensor. This tensor is axially-symmetric, large, and tends to align along the X-^{2}H bond, enabling for straightforward analysis. It has also been extensively used to study the dynamics of surface sites [12–20]. Dipolar coupling tensors are also frequent probes of motions [21–24], including from surface sites [25–27], and share many of the useful properties of the ^{2}H quadrupolar coupling tensor.

For studies of heterogeneous catalysts, there is tremendous value in the development of dynamic NMR methods that do not require isotope enrichment. To this end, some of us have investigated the applicability of ^{1}H CSA as a high-sensitivity dynamics probe [28]. Unfortunately, it was determined that challenges with estimating tensor orientation, magnitude, and asymmetry greatly limited its practicality. ^{1}H-^{1}H dipolar coupling strengths could also be applied to measure dynamics, however, their quantitative measurement is complicated by long-range interactions. Agarwal has addressed this problem in the case of unlike ^{1}H spins through the development of doubly band-selective methods which have been applied to extract distance restraints in proteins [29–32].

An ideal ^{1}H-^{1}H dipolar coupling-based dynamics probe would be a methylene. The intra-CH_2 dipolar coupling strength has a nearly constant magnitude and a well-defined orientation. Band-selective methods that require the two protons to have disparate chemical shifts, however, are not applicable to a methylene. Its relatively large magnitude, however, means that it can be measured using simpler schemes. Kobayashi *et al.*, for instance, recently used double-quantum spinning sidebands under fast-magic-angle spinning (MAS) conditions to measure the intra-CH_2 ^{1}H-^{1}H dipolar couplings for a silica surface-supported site [26]. Their method leveraged the back-to-back (BaBa) double-quantum recoupling sequence [33,34] most commonly used to acquire 2D double quantum/single quantum (DQ/SQ) correlation spectra. When the DQ evolution period is incremented in a rotor asynchronous manner, however, the sequence generates sideband patterns

that are proportional to the recoupled dipolar interaction's magnitude [35–38] and insensitive to other anisotropic interactions, such as chemical shift anisotropy [39]. This makes it particularly useful for the measurement of very strong dipolar couplings, such as short-range ^{1}H-^{1}H couplings.

Despite utilizing exclusively ^{1}H spins, the BaBa DQ sideband method is time intensive. Spinning sidebands are separated by twice the MAS spinning frequency ($2\nu_r$), which can require spectral windows in excess of 1 MHz in breadth while also maintaining chemical shift resolution (<100 Hz), thus necessitating the acquisition of thousands of t_1 increments. Herein we develop a frequency-selective (fs)BaBa sideband method that enables the rapid measurement of the dynamics of CH_2-containing moieties by eliminating the need for chemical shift resolution along the DQ dimension. The described strategy utilizes the selective inversion of the intra-CH_2 DQ transition [40] using rotor-synchronized delays alternating with nutations for tailored excitation (DANTE) pulses [41–45]. The resulting method considerably reduces the barriers to the measurement of the motions of surface sites.

2. Experimental

Malonic acid was purchased from Fisher Scientific and used as-is. The synthesis of allyl- and benzyl-functionalized mesoporous silica nanoparticles (Al-MSN and Bz-MSN) were described in earlier publications [46,47].

All experiments were performed on a Bruker Avance NEO 600 MHz solid-state NMR spectrometer equipped with a Varian 1.6 mm fast-MAS probe. All BaBa experiments utilized the xy-16 supercycle [34] with 100 kHz ^{1}H radiofrequency pulses. The MAS spinning frequencies were set to 40 kHz for malonic acid and Al-MSN and 35.714 kHz for Bz-MSN for which we could not achieve stable 40 kHz spinning. The number of 100 kHz DANTE pulses was optimized on each resonance and ranged from 25 to 100 pulses. No z-filter delay was used. Experiments were performed using recycle delays of 1, 1, and 2 s for malonic acid, Al-MSN, and Bz-MSN, respectively. 16 t_1 increments of $t_r/16$ were acquired for all fsBaBa sideband acquisitions, with each consisting of 32 scans. The excitation and reconversion recoupling times were set to 4 rotor periods for malonic acid and 6 rotor periods for Al-MSN and Bz-MSN. Uncertainties in the sideband intensities were estimated to equal the mean absolute noise level along the indirect dimension of the 2D spectrum. t_1-noise is the dominant source of noise and as such the uncertainties are most strongly correlated with the rotor stability and the number of spinning sidebands and not the overall sensitivity [48].

3. Theory

3.1. Averaging of Intra-CH_2 Dipolar Coupling Tensors

Nuclear spins interact through space via a direct dipolar coupling interaction with a magnitude characterized by the dipolar coupling constant (D).

$$D = \left(\frac{\mu_0}{4\pi}\right)\left(\frac{\gamma_1\gamma_2}{2\pi}\right)r^{-3} \quad (1)$$

In equation 1 μ_0 is the vacuum permeability, γ_n is the gyromagnetic ratio of nucleus 'n' and r is the internuclear distance between nuclei 1 and 2. This value is expected to be approximately 21 kHz for an intra-CH_2 ^{1}H-^{1}H spin pair when neglecting the averaging caused by vibrations and librations.

The orientational dependence of the interactions is represented by a traceless and axially-symmetric second rank tensor (**D**). In its principal axis system (PAS), i.e. with the ^{1}H-^{1}H internuclear vector oriented along the z direction, it is given by the following.

$$\mathbf{D}_{\mathrm{PAS}} = D\begin{bmatrix} 1 & 0 & 0 \\ 0 & 1 & 0 \\ 0 & 0 & -2 \end{bmatrix} \tag{2}$$

Here we will consider the impact caused by rotations about a leading X-CH_2 bond on this tensor. We will assume a constant ^{1}H-^{1}H distance, contained in a constant static D value. Note that the X-C bond is perpendicular to the ^{1}H-^{1}H internuclear vector in the CH_2 and can thus be oriented along the y direction. We can represent with rotation with the use of a Cartesian rotation matrix with a rotation axis aligned along the X-C bond ($\mathbf{R}_y$).

$$\mathbf{R}_y(\phi) = \begin{bmatrix} \cos\phi & 0 & -\sin\phi \\ 0 & 1 & 0 \\ \sin\phi & 0 & \cos\phi \end{bmatrix} \tag{3}$$

$$\mathbf{D}_{\mathrm{rot}}(\phi) = \mathbf{R}_y^{-1}(\phi)\mathbf{D}_{\mathrm{PAS}}\mathbf{R}_y(\phi) \tag{4}$$

$$\mathbf{D}_{\mathrm{rot}}(\phi) = D\begin{bmatrix} \cos^2\phi - 2\sin^2\phi & 0 & -3\cos\phi\sin\phi \\ 0 & 1 & 0 \\ -3\cos\phi\sin\phi & 0 & \sin^2\phi - 2\cos^2\phi \end{bmatrix} \tag{5}$$

If we assume that there is equal probability of the CH_2 to have a X-CH_2 bond dihedral deviation of ϕ or -ϕ from its lowest energy conformation (i.e. that the ϕ probability distribution is symmetric, see **Fig. 1a**) then the resulting 2-site exchanged dipolar coupling tensor is diagonal.

$$\mathbf{D}_{2-\mathrm{site}}(\phi) = (\mathbf{D}_{\mathrm{rot}}(\phi) + \mathbf{D}_{\mathrm{rot}}(-\phi))/2 \tag{6}$$

$$\mathbf{D}_{2-\mathrm{site}}(\phi) = D\begin{bmatrix} \frac{1}{2}(3\cos 2\phi - 1) & 0 & 0 \\ 0 & 1 & 0 \\ 0 & 0 & -\frac{1}{2}(3\cos 2\phi + 1) \end{bmatrix} \tag{7}$$

As such, from the 2-site exchange between two X-CH_2 bond rotation angles, we obtain a dynamically-averaged dipolar coupling tensor ($\mathbf{D}_{2\text{-site}}$) with principal components of D, D/2(3cos2ϕ - 1) and D/2(3cos2ϕ + 1). These dynamically-averaged principal components, $\langle D_{\mathrm{nn}}\rangle$, are generally re-ordered as: $|\langle D_{33}\rangle| \geq |\langle D_{22}\rangle| \geq |\langle D_{11}\rangle|$. The factor by which $\langle D_{33}\rangle$ is reduced relative to the static value, 2D, is known as the order parameter, $\langle S\rangle$. Evaluation of the expressions for the

principal components reveals that the order parameter oscillates from 1 to 0.5, depending on the value of ϕ.

$$\langle S \rangle = \left| \frac{\langle D_{33} \rangle}{2D} \right| \tag{8}$$

Dynamics may also lead to a non-zero dipolar asymmetry [49], quantified by an asymmetry parameter η_D, which ranges from 0, in an axially-symmetric tensor, to 1.

$$\eta_D = \frac{D_{11} - D_{22}}{D_{33}} \tag{9}$$

We, however, do not expect methylene groups to undergo 2-site exchange, but rather undergo Gaussian librational motions. We can adapt equation 5 to calculate the dynamically-averaged principal components, and thus the order parameter, for librations by integrating them over a Gaussian distribution of ϕ with a width of $\Delta\phi$[50,51].

$$P(\phi, \Delta\phi) = \sqrt{\frac{4\ln 2}{\pi}} \frac{1}{\Delta\phi} \exp\left(\frac{-4\phi^2 \ln 2}{\Delta\phi}\right) \tag{10}$$

In this case, the dynamically-averaged intra-CH_2 dipolar coupling tensor principal components can be calculated numerically as follows and the order parameter is calculated as described in equation 8.

$$\langle D_{nn} \rangle (\Delta\phi) = \int_{-\pi}^{\pi} P(\phi, \Delta\phi) \langle D_{nn} \rangle (\phi) d\phi \tag{11}$$

The dependence of $\langle S \rangle$ and η_D on the amplitude of the librations is depicted in **Fig. 1c,d**. Higher-amplitude librations lead to a monotonic decrease in $\langle S \rangle$ until $\Delta\phi = \pi/2$ after which it plateaus to a value of 0.5, corresponding to the $\langle D_{33} \rangle$ component being oriented along the X-C bond, unaffected by the librations. For low amplitude librations we thus expect $\langle S \rangle$ values ranging from 1 to 0.5. The observation of a value below 0.5 would indicate that a second dynamic mode is present in the sample, such as librations about two leading single bonds.

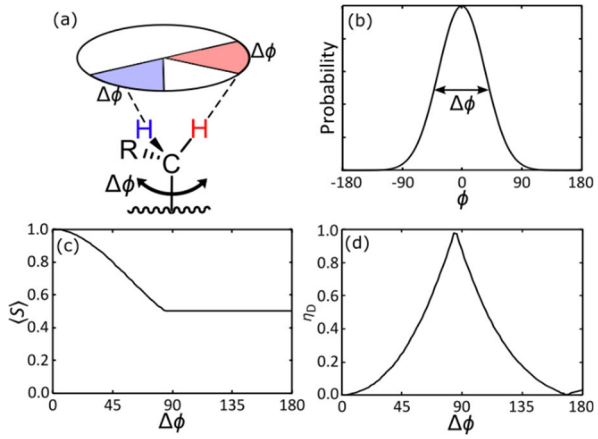

Fig. 1. (a) Illustration of librational dynamics of a CH_2. (b) Gaussian probability distribution of the dihedral angle ϕ, describing the amplitude of the librations. (c) Intra-CH_2 ^{1}H-^{1}H dipolar order parameter and (d) asymmetry parameter as a function of librational amplitude.

3.2. fsBaBa Pulse Sequence

One of the more common experiments that utilizes homonuclear dipolar recoupling is the double-quantum/single-quantum (DQ/SQ) correlation experiment. This experiment utilizes rotor-synchronized pulse sequences that generate a double-quantum average Hamiltonian to excite DQ coherences that can be detected indirectly in a 2D NMR experiment. The experiment reveals which sites are spatially proximate, albeit quantitative distance information is typically lost. The DQ build-up times can be used to estimate weak dipolar couplings in certain cases [35], however, the DQ sidebands are preferred for the measurement of strong dipolar couplings, such as those between the two ^{1}H spins of a methylene.

Dipolar coupling sensitive DQ sidebands are available if a γ-dependent dipolar recoupling sequence, such as BaBa [33,34], is used. We chose to apply the popular BaBa-xy16 sequence here, although the frequency-selection approach is transferable to other recoupling sequences [38,39,52,53]. BaBa is a non γ-encoded sequence that recouples DQ dipolar terms with space and spin components: $m = \pm 1$ and $\mu = \pm 2$ [54]. This indicates that efficient refocusing of the recoupled dipolar interactions is achieved when t_1 is a multiple of $t_r/2$ [55]. As such, the signal evolution along t_1 will have a beat frequency equal to $2\nu_r$ and odd-ordered spinning sidebands will be produced if t_1 is incremented in a non-rotor synchronized manner. The number of spinning sidebands that are produced will depend on the dipolar phase accumulation created during the recoupling and is thus proportional to $Dt_{rec}/2\pi$, with values from 0.5 to 1 being ideal to measure D [56].

If multiple resonances are present in the DQ/SQ correlation spectrum, then it is necessary to acquire very large numbers of t_1 increments to distinguish the spinning sideband patterns associated with distinct pairs of signals. Consider for instance that you wish to resolve the sideband patterns from two DQ signals separated by 1 ppm at 600 MHz (600 Hz), are spinning at 50 kHz, and expect 5 sidebands on either side of the spectrum. The spectral window along the indirect dimension would then need to equal 1 MHz and a minimum of 1700 t_1 increments would be required. In contrast, if chemical shift resolution were not required along the indirect dimension, then only 20 t_1 points would be required, corresponding to an 85-fold reduction in experiment time.

The same result could be achieved using a frequency-selective BaBa experiment. Here, we took inspiration from the strategies used to collect DQ/SQ correlation spectra correlating exclusively the central transitions of quadrupolar nuclei [57–59]. In these experiments, a central-transition selective inversion pulse is applied after DQ excitation to perform a selective $\pm 2 \rightarrow \mp 2$ coherence transfer and eliminate the intraspin DQ coherences that may have been excited during the dipolar recoupling. A similar strategy was recently applied to excite a 3-spin ^{11}B 3Q coherence

[60]. Like-spin DQ correlation, such as those between the two ^{1}H spins of a methylene, could similarly be selectively excited using a frequency-selective inversion pulse. Our fsBaBa pulse sequence is depicted in **Fig. 2** where we have inserted a DANTE [41–45] inversion pulse to perform the frequency-selective $\pm 2 \rightarrow \mp 2$ coherence transfer. This DANTE pulse has a total duration of n rotor periods/pulses with each pulse applying a 180°/n tip angle.

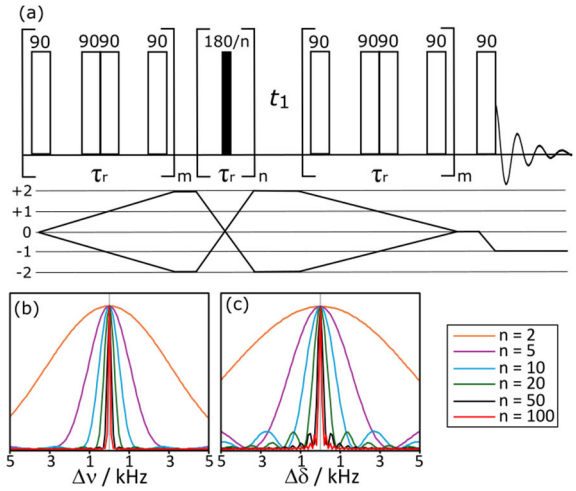

Fig. 2. (a) fsBaBa pulse sequence and coherence transfer pathway. We applied a 32-step phase cycle wherein the phases of the first recoupling cycle and the final 90° pulse were cycled in 4 steps while the DANTE pulse was cycled in two steps (0°, 45°) with a commensurate inversion of the transmitter phase. The BaBa pulses are cycled using the xy-16 supercycle [34]. SIMPSON simulations of the efficiency of the DQ reconversion as a function of the transmitter offset (b) and resonance separation (c) for the values of 'n' described on the Figure.

The performance of the DANTE selection pulse was evaluated using SIMPSON numerical simulations [61,62] of a simple, dipolar-coupled, 2-spin system with a dipolar coupling constant equal to 21 kHz (**Fig. 2b,c**). The plots in **Fig. 2b** display the effect of shifting the transmitter offset on the DQ reconversion efficiency for an increasing number of DANTE pulse segments (n), assuming two ^{1}H nuclei with identical chemical shifts. In contrast, the plots in **Fig. 2c** show that similar selection from the DANTE pulse is obtained if the chemical shift difference between the two recoupled sites is nonzero.

Given that a fast Fourier transform will be applied to process the spectra, t_1 should be incremented in $N=2^m$ steps of t_r/N. This will reveal N/4 unique DQ spinning sidebands, with 1 datum per ν_r frequency offset. In this study we acquired 16 t_1 increments for the fsBaBa spectra, which yields four positive and negative spinning sidebands.

4. Results and Discussion

In the following sections we evaluate the performance of the fsBaBa sequence for determining strong like-spin dipolar coupling constants using malonic acid's CH_2 as a model system. We subsequently use the sequence to characterize the dynamics occurring in two silica-supported species. Experimental sideband patterns are fitted using SIMPSON simulations of simple 2-spin models using identical conditions as those used in the experiments.

4.1. Malonic Acid

To test whether the fsBaBa sequence can measure accurate like-spin dipolar coupling constants we selected malonic acid. This compound possesses a rigid structure with a spectrally-resolved methylene signal. The ^{1}H NMR spectrum contains two signals from the central methylene and the terminal carboxylic acid moieties at 2.4 and 12.3 ppm, respectively.

Matching the transmitter frequency to that of the methylene resonance, we evaluated the frequency selection from the DANTE pulse. The dependence of the DQ-filtered ^{1}H NMR spectra as a function of the number of DANTE inversion pulse segments (n) is shown in **Fig. 3a**. We observed a rapid elimination of the unwanted acid-correlated DQ signals after only five segments, suggesting that the required number of segments to select a signal from a pair separated by $\Delta\delta$ is empirically approximated by:

$$\mathrm{n} = \frac{\nu_r}{40\ \mathrm{kHz}} \frac{50\ ppm}{\Delta\delta}. \qquad (10)$$

2D DQ/SQ correlation spectra acquired with the fsBaBa sequence and n values of 1 and 10 are shown in **Fig. 3b**, with the n = 10 spectra also being acquired with the transmitter positioned on either signal. From these correlation spectra we can ascertain that the sequence is behaving as designed and is indeed selecting only a single like-spin DQ correlation. Intensity losses that result from decoherence during the DANTE train were moderate at 42 and 64% reductions when n = 5 and 10, respectively. Some of these intensity losses are nevertheless desired as they originate from the elimination of intersite correlations. The double-quantum filtering efficiency, as compared to a Hahn echo experiment, was 0.6%.

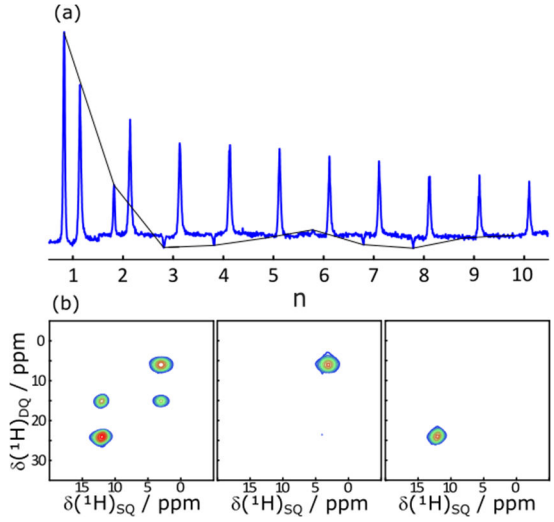

Fig. 3. (a) Optimization of the number of DANTE pulse segments for the methylene signal of malonic acid (ν_r = 40 kHz). (b) 2D DQ/SQ correlation spectra acquired with n=1 (left) and n=10 (center and right) with the transmitter placed on either signal.

DQ sideband patterns were acquired selecting either of the ^{1}H NMR signals in malonic acid to measure their dipolar coupling constants (**Fig. 4**). The CH_2 DQ sideband pattern was best fit to a *D* value of 17.7 kHz. This value is lower than the expected value of 21 kHz from a typical methylene, likely due to low-amplitude motions such as C-H stretching and H-C-H bending modes. These factors are expected to be present in for all methylenes and as such, a value of 17.7 kHz will be used to approximate the static *D* value for the remainder of this study.

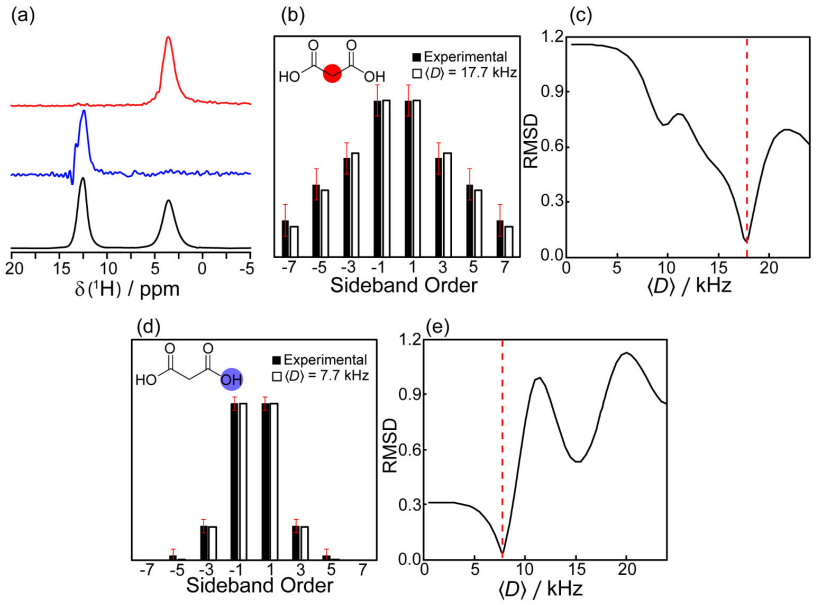

Fig. 4. (a) DQ-filtered ^{1}H fast-MAS NMR spectra of malonic acid acquired without any frequency selection (bottom, black) and with the selection of the methylene (red, top) and carboxyl (blue, middle) signals. Experimental (black) and simulated (white) normalized DQ sideband patterns for the CH_2 (b) and COOH (d) signals. Plots of the RMSD between the experimental and SIMPSON-calculated sideband patterns are shown in (c) and (e) for the same respective signals as a function of *D*. Red dashed lines indicate the dipolar coupling value best fit.

The acid groups of malonic acid form hydrogen bonded pairs in the solid state [63] and as such the COOH-COOH ^{1}H-^{1}H dipolar coupling constant is sizeable and expected to be of approximately 8-9 kHz. Its DQ sideband pattern is shown in **Fig. 4** and is best-fitted to a *D* value of 7.7 kHz, in agreement with the crystal structure when also considering vibrational averaging.[64] We can thus conclude that the fsBaBa experiment should enable for the rapid and sensitive estimation of dynamics involving CH_2 moieties. In the following sections we apply it to the study of the motions of surface-supported sites.

4.2. Allyl-Functionalized Mesoporous Silica

Recently, the dynamics of silica-supported allyl moieties in Al-MSN were evaluated using the conventional BaBa DQ sideband experiment, with the primary goal of evaluating intersite distances [26]. We have thus selected the Al-MSN sample as the ideal first sample to test the fsBaBa method. The allyl moieties contain two CH_2 groups that enable us to probe dynamics across both of the moiety's single C-C bonds.

The sideband patterns measured by selecting either of the methylene signals are shown in **Fig. 5**. Narrower sideband patterns than observed in malonic acid were detected, in agreement with the presence of motions. In the case of the α-CH_2, we measured a 10.2 kHz $\langle D \rangle$ value, corresponding to an order parameter of 0.58 or, equivalently, a librational amplitude ($\Delta\phi$) of approximately 72°. This amplitude is in good agreement with that predicted by Kobayashi *et al.* [26] using molecular dynamics simulations.

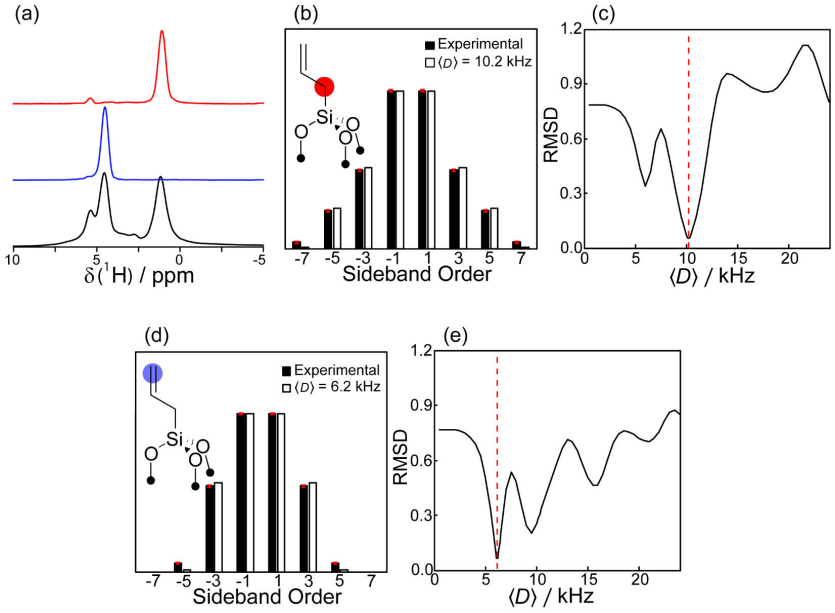

Fig. 5. (a) DQ-filtered ^{1}H fast-MAS NMR spectra of Al-MSN acquired without any frequency selection (bottom, black) and with the selection of the Si-CH_2 (red, top) and terminal CH_2 (blue, middle) signals. Experimental (black) and simulated (white) normalized DQ sideband patterns for the Si-CH_2 (b) and terminal CH_2 (d) signals. Plots of the RMSD between the experimental and SIMPSON-calculated sideband patterns are shown in (c) and (e) for the same respective signals as a function of *D*. Red dashed lines indicate the dipolar coupling value best fit.

The γ-CH_2 $\langle D \rangle$ value is a further averaged to 6.2 kHz, equating to a $\langle S \rangle$ value of 0.35. As expected, the dynamics across both single bonds are compounded and a $\langle S \rangle$ value below the single-dynamic mode limit of 0.5 is produced. The fact that this value is nearly equal to the square of the value measured for the α-CH_2 suggests a similar librational amplitude of ~72° is available across both single bonds.

4.3. Benzyl-Functionalized Mesoporous Silica

We lastly study the structurally-related benzyl-functionalized silica (Bz-MSN). Given the bulkier nature of the phenyl moiety in Bz-MSN, as compared to the ethenyl moiety in Al-MSN, we would expect the former to undergo lower amplitude motions. We measured the DQ sideband patterns for both the methylene and phenyl signals using the fsBaBa sequence. These are depicted in **Fig. 6** together with their numerical fits. We measured a CH_2 $\langle D \rangle$ value of 10.8 kHz, corresponding to $\langle S \rangle = 0.61$. While this value is somewhat larger than that measured in Al-MSN, it corresponds only to a slight reduction in the librational amplitude from 72° to 69° from the increased sterics, suggesting that the phenyl group is not sufficiently large to lock the group's orientation on the surface

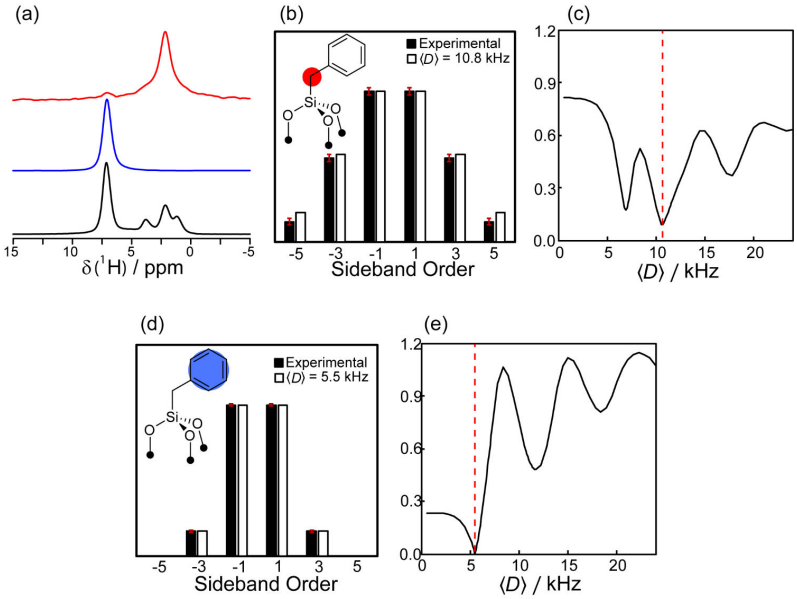

Fig. 6. (a) DQ-filtered ^{1}H fast-MAS NMR spectra of Bz-MSN acquired without any frequency selection (bottom, black) and with the selection of the Si-CH_2 (red, top) and aromatic (blue, middle) signals. Experimental (black) and simulated (white) normalized DQ sideband patterns for the Si-CH_2 (b) and aromatic (d) signals. Plots of the RMSD between the experimental and SIMPSON-calculated sideband patterns are shown in (c) and (e) for the same respective signals as a function of *D*. Red dashed lines indicate the dipolar coupling value best fit.

In the case of the phenyl resonance, at this MAS frequency, the *ortho*-, *meta*-, and *para*-^{1}H NMR signals are not resolved. As such, the experiment should primarily report on the strength of the nearest neighbor dipolar couplings (*ortho-meta* and *meta-para*), which are expected to equal 7.8 kHz. From the experimental sideband pattern, we obtained a $\langle D \rangle$ value of 5.5 kHz, corresponding to an intra-Ph $\langle S \rangle$ value of 0.70. This relatively large value indicates that while there is significant freedom along the Si-CH_2 bond, the CH_2-Ph librational dynamics are comparatively restricted.

5. Conclusions

We designed a frequency-selective variant of the double-quantum sideband method used for the measurement of homonuclear dipolar coupling strengths. The pulse sequence uses a DANTE pulse to perform a selective $\pm 2 \rightarrow \mp 2$ coherence transfer and isolate a single like-spin double quantum coherence. Given dramatic reductions in the required number of t_1 increments, this experiment reduces the time needed to measure strong ^{1}H-^{1}H dipolar coupling constants by two orders of magnitude.

We discussed the applicability of this method for studies of dynamics in difficult to isotopically-enrich samples, such as heterogeneous catalysts. In these cases, the well-defined intra-CH_2 ^{1}H-^{1}H dipolar coupling can be leveraged as a dynamics probe. We elaborated on how this dipolar coupling is impacted by librational and rotational dynamics and specify how it can be further used to reveal combined motions. This methodology was applied to study the motions of silica-supported allyl and benzyl moieties and the impacts of increased sterics on the motions of surface sites.

Acknowledgements

This work was supported by the U.S. Department of Energy (DOE), Office of Basic Energy Sciences, Division of Chemical Sciences, Geosciences, and Biosciences through a DOE Early Career Project. Ames National Laboratory is operated for the DOE by Iowa State University under Contract No. DE-AC02-07CH11358.

References

[1] H. Zhai, A.N. Alexandrova, Local Fluxionality of Surface-Deposited Cluster Catalysts: The Case of Pt_7 on Al_2O_3, J. Phys. Chem. Lett. 9 (2018) 1696–1702. https://doi.org/10.1021/acs.jpclett.8b00379.

[2] H. Zhai, A.N. Alexandrova, Fluxionality of Catalytic Clusters: When It Matters and How to Address It, ACS Catal. 7 (2017) 1905–1911. https://doi.org/10.1021/acscatal.6b03243.

[3] B. Zandkarimi, A.N. Alexandrova, Dynamics of Subnanometer Pt Clusters Can Break the Scaling Relationships in Catalysis, J. Phys. Chem. Lett. 10 (2019) 460–467. https://doi.org/10.1021/acs.jpclett.8b03680.

[4] K.F. Kalz, R. Kraehnert, M. Dvoyashkin, R. Dittmeyer, R. Gläser, U. Krewer, K. Reuter, J.-D. Grunwaldt, Future Challenges in Heterogeneous Catalysis: Understanding Catalysts under Dynamic Reaction Conditions, ChemCatChem 9 (2017) 17–29. https://doi.org/10.1002/cctc.201600996.

[5] J. Guo, H.-X. Zhou, Protein Allostery and Conformational Dynamics, Chem. Rev. 116 (2016) 6503–6515. https://doi.org/10.1021/acs.chemrev.5b00590.

[6] A. Kohen, Role of Dynamics in Enzyme Catalysis: Substantial versus Semantic Controversies, Acc. Chem. Res. 48 (2015) 466–473. https://doi.org/10.1021/ar500322s.

[7] O. Rivoire, Geometry and Flexibility of Optimal Catalysts in a Minimal Elastic Model, J. Phys. Chem. B 124 (2020) 807–813. https://doi.org/10.1021/acs.jpcb.0c00244.

[8] B.R. Goldsmith, B. Peters, J.K. Johnson, B.C. Gates, S.L. Scott, Beyond Ordered Materials: Understanding Catalytic Sites on Amorphous Solids, ACS Catal. 7 (2017) 7543–7557. https://doi.org/10.1021/acscatal.7b01767.
[9] A. Mittermaier, L.E. Kay, New Tools Provide New Insights in NMR Studies of Protein Dynamics, Science 312 (2006) 224–228. https://doi.org/10.1126/science.1124964.
[10] A. Sekhar, L.E. Kay, An NMR View of Protein Dynamics in Health and Disease, Annu. Rev. Biophys. 48 (2019) 297–319. https://doi.org/10.1146/annurev-biophys-052118-115647.
[11] J.J. Kinnun, A. Leftin, M.F. Brown, Solid-State NMR Spectroscopy for the Physical Chemistry Laboratory, J. Chem. Educ. 90 (2013) 123–128. https://doi.org/10.1021/ed2004774.
[12] J. Gath, G.L. Hoaston, R.L. Vold, R. Berthoud, C. Copéret, M. Grellier, S. Sabo-Etienne, A. Lesage, L. Emsley, Motional heterogeneity in single-site silica-supported species revealed by deuteron NMR, Phys. Chem. Chem. Phys. 11 (2009) 6962–6971. https://doi.org/10.1039/B907665D.
[13] A.D. Nicola, A. Correa, S. Bracco, J. Perego, P. Sozzani, A. Comotti, G. Milano, Collective Dynamics of Molecular Rotors in Periodic Mesoporous Organosilica: A Combined Solid-State ^{2}H-NMR and Molecular Dynamics Simulation Study, Phys. Chem. Chem. Phys. 24 (2022) 666–673. https://doi.org/10.1039/D1CP05013C.
[14] S. Bracco, A. Comotti, P. Valsesia, B.F. Chmelka, P. Sozzani, Molecular rotors in hierarchically ordered mesoporous organosilica frameworks, Chem. Commun. (2008) 4798–4800. https://doi.org/10.1039/B809559K.
[15] T. Kobayashi, J.A. DiVerdi, G.E. Maciel, Silica Gel Surface: Molecular Dynamics of Surface Silanols, J. Phys. Chem. C 112 (2008) 4315–4326. https://doi.org/10.1021/jp709759e.
[16] M. Weigler, M. Brodrecht, H. Breitzke, F. Dietrich, M. Sattig, G. Buntkowsky, M. Vogel, ^{2}H NMR Studies on Water Dynamics in Functionalized Mesoporous Silica, Z. Für Phys. Chem. 232 (2018) 1041–1058. https://doi.org/10.1515/zpch-2017-1034.
[17] S. Jayanthi, V. Frydman, S. Vega, Dynamic Deuterium Magic Angle Spinning NMR of a Molecule Grafted at the Inner Surface of a Mesoporous Material, J. Phys. Chem. B 116 (2012) 10398–10405. https://doi.org/10.1021/jp3061152.
[18] Q. Wang, E. Jordan, D.F. Shantz, 2H NMR Studies of Simple Organic Groups Covalently Attached to Ordered Mesoporous Silica, J. Phys. Chem. C 113 (2009) 18142–18151. https://doi.org/10.1021/jp9013527.
[19] E. Steinrücken, T. Wissel, M. Brodrecht, H. Breitzke, J. Regentin, G. Buntkowsky, M. Vogel, ^{2}H NMR study on temperature-dependent water dynamics in amino-acid functionalized silica nanopores, J. Chem. Phys. 154 (2021) 114702. https://doi.org/10.1063/5.0044141.
[20] B. Boddenberg, R. Grosse, U. Breuninger, ^{2}H NMR spectra of trimethylsilyl groups anchored on a silica surface, Surf. Sci. 173 (1986) L655–L658. https://doi.org/10.1016/0039-6028(86)90193-7.
[21] S.A. Southern, F.A. Perras, Comparison of methods for the NMR measurement of motionally averaged dipolar couplings, J. Magn. Reson. 364 (2024) 107710. https://doi.org/10.1016/j.jmr.2024.107710.

[22] P. Schanda, M. Huber, J. Boisbouvier, B.H. Meier, M. Ernst, Solid-State NMR Measurements of Asymmetric Dipolar Couplings Provide Insight into Protein Side-Chain Motion, Angew. Chem. Int. Ed. 50 (2011) 11005–11009. https://doi.org/10.1002/anie.201103944.
[23] G. Hou, X. Lu, A.J. Vega, T. Polenova, Accurate measurement of heteronuclear dipolar couplings by phase-alternating R-symmetry (PARS) sequences in magic angle spinning NMR spectroscopy, J. Chem. Phys. 141 (2014) 104202. https://doi.org/10.1063/1.4894226.
[24] B.-J. van Rossum, C.P. de Groot, V. Ladizhansky, S. Vega, H.J.M. de Groot, A Method for Measuring Heteronuclear ($^{1}H-^{13}C$) Distances in High Speed MAS NMR, J. Am. Chem. Soc. 122 (2000) 3465–3472. https://doi.org/10.1021/ja992714j.
[25] S. Nedd, T. Kobayashi, C.-H. Tsai, I.I. Slowing, M. Pruski, M.S. Gordon, Using a Reactive Force Field To Correlate Mobilities Obtained from Solid-State ^{13}C NMR on Mesoporous Silica Nanoparticle Systems, J. Phys. Chem. C 115 (2011) 16333–16339. https://doi.org/10.1021/jp204510m.
[26] T. Kobayashi, D.-J. Liu, F.A. Perras, Spatial arrangement of dynamic surface species from solid-state NMR and machine learning-accelerated MD simulations, Chem. Commun. 58 (2022) 13939–13942. https://doi.org/10.1039/D2CC05861H.
[27] A.L. Paterson, D.-J. Liu, U. Kanbur, A.D. Sadow, F.A. Perras, Observing the three-dimensional dynamics of supported metal complexes, Inorg. Chem. Front. 8 (2021) 1416–1431. https://doi.org/10.1039/D0QI01241F.
[28] S.A. Southern, D.-J. Liu, P. Chatterjee, Y. Li, F.A. Perras, ^{1}H chemical shift anisotropy: a high sensitivity solid-state NMR dynamics probe for surface studies?, Phys. Chem. Chem. Phys. 25 (2023) 5348–5360. https://doi.org/10.1039/D2CP04406D.
[29] M.G. Jain, D. Lalli, J. Stanek, C. Gowda, S. Prakash, T.S. Schwarzer, T. Schubeis, K. Castiglione, L.B. Andreas, P.K. Madhu, G. Pintacuda, V. Agarwal, Selective $^{1}H–^{1}H$ Distance Restraints in Fully Protonated Proteins by Very Fast Magic-Angle Spinning Solid-State NMR, J. Phys. Chem. Lett. 8 (2017) 2399–2405. https://doi.org/10.1021/acs.jpclett.7b00983.
[30] L.R. Potnuru, N.T. Duong, S. Ahlawat, S. Raran-Kurussi, M. Ernst, Y. Nishiyama, V. Agarwal, Accuracy of $^{1}H–^{1}H$ distances measured using frequency selective recoupling and fast magic-angle spinning, J. Chem. Phys. 153 (2020) 084202. https://doi.org/10.1063/5.0019717.
[31] N.T. Duong, S. Raran-Kurussi, Y. Nishiyama, V. Agarwal, Quantitative $^{1}H–^{1}H$ Distances in Protonated Solids by Frequency-Selective Recoupling at Fast Magic Angle Spinning NMR, J. Phys. Chem. Lett. 9 (2018) 5948–5954. https://doi.org/10.1021/acs.jpclett.8b02189.
[32] S. Ahlawat, S.M.V. Mopidevi, P.P. Taware, S. Raran-Kurussi, K.R. Mote, V. Agarwal, Assignment of aromatic side-chain spins and characterization of their distance restraints at fast MAS, J. Struct. Biol. X 7 (2023) 100082. https://doi.org/10.1016/j.yjsbx.2022.100082.
[33] M. Feike, D.E. Demco, R. Graf, J. Gottwald, S. Hafner, H.W. Spiess, Broadband Multiple-Quantum NMR Spectroscopy, J. Magn. Reson. A 122 (1996) 214–221. https://doi.org/10.1006/jmra.1996.0197.

[34] K. Saalwächter, F. Lange, K. Matyjaszewski, C.-F. Huang, R. Graf, BaBa-xy16: Robust and broadband homonuclear DQ recoupling for applications in rigid and soft solids up to the highest MAS frequencies, J. Magn. Reson. 212 (2011) 204–215. https://doi.org/10.1016/j.jmr.2011.07.001.
[35] K. Saalwächter, Robust NMR approaches for the determination of homonuclear dipole-dipole coupling constants in studies of solid materials and biomolecules, Chemphyschem Eur. J. Chem. Phys. Phys. Chem. 14 (2013) 3000–3014. https://doi.org/10.1002/cphc.201300254.
[36] I. Schnell, A. Watts, H. Spiess, Double-quantum double-quantum MAS exchange NMR spectroscopy: Dipolar-coupled spin pairs as probes for slow molecular dynamics, J. Magn. Reson. 149 (2001). https://ora.ox.ac.uk/objects/uuid:cb337a7d-7329-4abc-b711-4feb7191c19d (accessed November 29, 2024).
[37] I. Schnell, H.W. Spiess, High-Resolution ^{1}H NMR Spectroscopy in the Solid State: Very Fast Sample Rotation and Multiple-Quantum Coherences, J. Magn. Reson. 151 (2001) 153–227. https://doi.org/10.1006/jmre.2001.2336.
[38] R. Graf, D.E. Demco, J. Gottwald, S. Hafner, H.W. Spiess, Dipolar couplings and internuclear distances by double-quantum nuclear magnetic resonance spectroscopy of solids, J. Chem. Phys. 106 (1997) 885–895. https://doi.org/10.1063/1.473169.
[39] A. Brinkmann, M. Edén, Central-transition double-quantum sideband NMR spectroscopy of half-integer quadrupolar nuclei: estimating internuclear distances and probing clusters within multi-spin networks, Phys. Chem. Chem. Phys. 16 (2014) 7037–7050. https://doi.org/10.1039/C4CP00029C.
[40] G. Mali, G. Fink, F. Taulelle, Double-quantum homonuclear correlation magic angle sample spinning nuclear magnetic resonance spectroscopy of dipolar-coupled quadrupolar nuclei, J. Chem. Phys. 120 (2004) 2835–2845. https://doi.org/10.1063/1.1638741.
[41] G. Goobes, E. Vinogradov, S. Vega, Selective polarization inversion of protons in rotating solids, J. Magn. Reson. 161 (2003) 56–63. https://doi.org/10.1016/S1090-7807(02)00135-0.
[42] G.A. Morris, R. Freeman, Selective excitation in Fourier transform nuclear magnetic resonance, J. Magn. Reson. 1969 29 (1978) 433–462. https://doi.org/10.1016/0022-2364(78)90003-3.
[43] G. Bodenhausen, R. Freeman, G.A. Morris, A simple pulse sequence for selective excitation in Fourier transform NMR, J. Magn. Reson. 1969 23 (1976) 171–175. https://doi.org/10.1016/0022-2364(76)90150-5.
[44] P. Caravatti, G. Bodenhausen, R.R. Ernst, Selective pulse experiments in high-resolution solid state NMR, J. Magn. Reson. 1969 55 (1983) 88–103. https://doi.org/10.1016/0022-2364(83)90279-2.
[45] V. Vitzthum, M.A. Caporini, S. Ulzega, G. Bodenhausen, Broadband excitation and indirect detection of nitrogen-14 in rotating solids using Delays Alternating with Nutation (DANTE), J. Magn. Reson. 212 (2011) 234–239. https://doi.org/10.1016/j.jmr.2011.06.013.

[46] S. Huh, J.W. Wiench, J.-C. Yoo, M. Pruski, V.S.-Y. Lin, Organic Functionalization and Morphology Control of Mesoporous Silicas via a Co-Condensation Synthesis Method, Chem. Mater. 15 (2003) 4247–4256. https://doi.org/10.1021/cm0210041.
[47] J.S. Valenstein, K. Kandel, F. Melcher, I.I. Slowing, V.S.-Y. Lin, B.G. Trewyn, Functional Mesoporous Silica Nanoparticles for the Selective Sequestration of Free Fatty Acids from Microalgal Oil, ACS Appl. Mater. Interfaces 4 (2012) 1003–1009. https://doi.org/10.1021/am201647t.
[48] Y. Nishiyama, V. Agarwal, R. Zhang, Efficient symmetry-based γ-encoded DQ recoupling sequences for suppression of *t*1-noise in solid-state NMR spectroscopy at fast MAS, Solid State Nucl. Magn. Reson. 114 (2021) 101734. https://doi.org/10.1016/j.ssnmr.2021.101734.
[49] P. Schanda, M. Huber, J. Boisbouvier, B.H. Meier, M. Ernst, Solid-State NMR Measurements of Asymmetric Dipolar Couplings Provide Insight into Protein Side-Chain Motion, Angew. Chem. Int. Ed. 50 (2011) 11005–11009. https://doi.org/10.1002/anie.201103944.
[50] F.A. Perras, U. Chaudhary, I.I. Slowing, M. Pruski, Probing Surface Hydrogen Bonding and Dynamics by Natural Abundance, Multidimensional, ^{17}O DNP-NMR Spectroscopy, J. Phys. Chem. C 120 (2016) 11535–11544. https://doi.org/10.1021/acs.jpcc.6b02579.
[51] F. Ragone, A. Poater, L. Cavallo, Flexibility of N-Heterocyclic Carbene Ligands in Ruthenium Complexes Relevant to Olefin Metathesis and Their Impact in the First Coordination Sphere of the Metal, J. Am. Chem. Soc. 132 (2010) 4249–4258. https://doi.org/10.1021/ja909441x.
[52] A. Brinkmann, M. Edén, Estimating internuclear distances between half-integer quadrupolar nuclei by central-transition double-quantum sideband NMR spectroscopy, Can. J. Chem. 89 (2011) 892–899. https://doi.org/10.1139/v11-020.
[53] J. Gottwald, D.E. Demco, R. Graf, H.W. Spiess, High-resolution double-quantum NMR spectroscopy of homonuclear spin pairs and proton connectivities in solids, Chem. Phys. Lett. 243 (1995) 314–323. https://doi.org/10.1016/0009-2614(95)00872-2.
[54] M.H. Levitt, Symmetry-Based Pulse Sequences in Magic-Angle Spinning Solid-State NMR, in: eMagRes, John Wiley & Sons, Ltd, 2007. https://doi.org/10.1002/9780470034590.emrstm0551.
[55] K. Märker, S. Hediger, G.D. Paëpe, Efficient 2D double-quantum solid-state NMR spectroscopy with large spectral widths, Chem. Commun. 53 (2017) 9155–9158. https://doi.org/10.1039/C7CC04890D.
[56] I. Schnell, A. Watts, H.W. Spiess, Double-Quantum Double-Quantum MAS Exchange NMR Spectroscopy: Dipolar-Coupled Spin Pairs as Probes for Slow Molecular Dynamics, J. Magn. Reson. 149 (2001) 90–102. https://doi.org/10.1006/jmre.2001.2290.
[57] G. Mali, G. Fink, F. Taulelle, Double-quantum homonuclear correlation magic angle sample spinning nuclear magnetic resonance spectroscopy of dipolar-coupled quadrupolar nuclei, J. Chem. Phys. 120 (2004) 2835–2845. https://doi.org/10.1063/1.1638741.
[58] Q. Wang, B. Hu, O. Lafon, J. Trébosc, F. Deng, J.P. Amoureux, Double-quantum homonuclear NMR correlation spectroscopy of quadrupolar nuclei subjected to

magic-angle spinning and high magnetic field, J. Magn. Reson. 200 (2009) 251–260. https://doi.org/10.1016/j.jmr.2009.07.009.
[59] M. Edén, D. Zhou, J. Yu, Improved double-quantum NMR correlation spectroscopy of dipolar-coupled quadrupolar spins, Chem. Phys. Lett. 431 (2006) 397–403. https://doi.org/10.1016/j.cplett.2006.09.081.
[60] F.A. Perras, H. Thomas, P. Heintz, R. Behera, J. Yu, G. Viswanathan, D. Jing, S.A. Southern, K. Kovnir, L. Stanley, W. Huang, The Structure of Boron Monoxide, J. Am. Chem. Soc. 145 (2023) 14660–14669. https://doi.org/10.1021/jacs.3c02070.
[61] Z. Tošner, R. Andersen, B. Stevensson, M. Edén, N.C. Nielsen, T. Vosegaard, Computer-intensive simulation of solid-state NMR experiments using SIMPSON, J. Magn. Reson. 246 (2014) 79–93. https://doi.org/10.1016/j.jmr.2014.07.002.
[62] M. Bak, J.T. Rasmussen, N.C. Nielsen, SIMPSON: A General Simulation Program for Solid-State NMR Spectroscopy, J. Magn. Reson. 147 (2000) 296–330. https://doi.org/10.1006/jmre.2000.2179.
[63] J.A. Goedkoop, C.H. MacGillavry, The Crystal Structure of Malonic Acid, Acta Crystallogr. 10 (1957) 125–127. https://doi.org/10.1107/S0365110X57000353.
[64] G. Wu, I. Hung, Z. Gan, V. Terskikh, X. Kong, Solid-State ^{17}O NMR Study of Carboxylic Acid Dimers: Simultaneously Accessing Spectral Properties of Low- and High-Energy Tautomers, J. Phys. Chem. A 123 (2019) 8243–8253. https://doi.org/10.1021/acs.jpca.9b07224.